

Orbital order and fluctuation in BaFe_2X_3 ($X = \text{S}$ and Se) and CsFe_2Se_3 probed by x-ray absorption and resonant inelastic x-ray scattering spectroscopy

Kou Takubo,^{1,*} Yuichi Yokoyama,¹ Hiroki Wadati,¹ Takashi Mizokawa,² Teak Boyko,³ Ronny Sutarto,³ Feizhou He,³ Kazuki Hashizume,⁴ Takuya Aoyama,⁴ and Kenya Ohgushi⁴

¹*Institute for Solid State Physics, University of Tokyo, Kashiwa, Chiba 277-8581, Japan*

²*Department of Applied Physics, Waseda University, Okubo 277-8581, Japan*

³*Canadian Light Source, Saskatoon, Saskatchewan S7N 0X4, Canada*

⁴*Department of Physics, Tohoku University, Sendai 980-8578, Japan*

(Dated: December 3, 2024)

The electronic structure of BaFe_2X_3 ($X = \text{S}$ and Se) and CsFe_2Se_3 in which two-leg ladders are formed by the Fe sites are studied by means of x-ray absorption and resonant inelastic x-ray scattering spectroscopy. The x-ray absorption spectra at the Fe L edges for BaFe_2X_3 exhibit two components, indicating that itinerant and localized Fe $3d$ sites coexist. Substantial x-ray linear dichroism (XLD) is observed in polarization dependent spectra, indicating the existence of orbital order or fluctuation in the Fe-ladder even above the Néel temperature T_N . Direct exchange interaction along the legs of the Fe-ladder stabilizes the orbital and antiferromagnetic orders in BaFe_2S_3 , while the ferromagnetic molecular orbitals are realized between the rungs in CsFe_2Se_3 .

PACS numbers: 78.70.Dm, 78.70.En, 74.70.Xa, 75.25.Dk

The magnetic-orbital fluctuations and their anisotropies in iron-based superconductors have been attracting much attention. The parent compounds of the iron-based superconductors show antiferromagnetic (AF) transitions at low temperatures, typically exhibiting striped-type magnetic ordering. On the basis of theoretical analyses on multi-band models with hole and electron Fermi pockets, the striped-type magnetic ordering is stabilized by Fermi-surface nesting, and the associated AF and orbital fluctuations are proposed to induce the superconductivity [1–6]. However, there are some iron-based superconductors showing significant disagreement with the Fermi-surface nesting scenario. For example, superconductivity with $T_c \sim 30$ K in $\text{A}_2\text{Fe}_4\text{Se}_5$ ($A = \text{K}, \text{Rb}, \text{and Cs}$) [7–9] appears in the vicinity of Mott insulating state with block-type AF ordering. In this context, it is very important to study the nature of the Mott insulating state in the parent compounds of iron-based superconductors.

Recently, another insulating Fe chalcogenide AFe_2X_3 ($A = \text{Cs}$ and Ba , $X = \text{S}$ and Se) has been attracting attention due to the specific quasi-one-dimensional crystal structure and magnetism [10–25]. In this family of compounds, $\text{Fe}(\text{S}, \text{Se})_4$ tetrahedra share their edges and form a two-leg ladder of Fe sites as shown in Fig. 1 (a). These compounds all exhibit unique magnetic ordering. The magnetic structure of BaFe_2Se_3 ($Pnma$ space group) is a one-dimensional analogue of the block magnetism observed in $\text{A}_2\text{Fe}_4\text{Se}_5$, in that four Fe spins in the two-leg ladder form a ferromagnetic block and the neighboring blocks are antiferromagnetically coupled as illustrated in Fig. 1 (f) [11–14]. In contrast, the magnetic structures of BaFe_2S_3 and CsFe_2Se_3 ($Cmcm$ space group), are of the stripe-type, in which the magnetic moments couple ferromagnetically along the rung, and antiferromagnetically

along the leg direction [15, 16]. However, the magnetic moments in CsFe_2Se_3 point toward the layers, while those in BaFe_2S_3 point toward the rungs.

Moreover, recent works under high-pressures revealed that BaFe_2S_3 , which is the most conductive compound among these compounds, shows an appearance of the superconducting phase at $T_c \sim 14$ K under 11 GPa without major crystal structure change [17]. Also it has been clarified that the superconducting phase is in the vicinity of bandwidth-control type Mott transition [18]. In addition, the magnetic transition temperature and resistivity of BaFe_2X_3 (Fe^{2+}) depend on the sample stoichiometry. Lei *et al.* reported the activation-type temperature dependence for BaFe_2Se_3 with a band gap of 0.18 eV [19]. On the other hand, one-dimensional variable range hopping was reported, indicating that some carriers are localized due to strong scattering effects in the quasi-one-dimensional structure [14, 18, 20]. In addition, coexistence of the itinerant and localized electrons was indicated by the resonant inelastic x-ray scattering (RIXS) [21], and x-ray photoemission spectroscopy (XPS) [22]. These observations suggest that the itinerant electrons introduced by small Fe vacancies or some other effects would be responsible for the variable range-hopping behaviour of the resistivity [14, 18, 20]. In contrast to BaFe_2X_3 , CsFe_2Se_3 with formal Fe valence of +2.5 is much more insulating. Usually, Mott insulators with integer number of valence are expected to be more insulating than the mixed valence systems. Such puzzling mismatch between the formal valence and the transport behaviour indicates unusual electronic states in the vicinity of the superconducting phase of AFe_2X_3 . The x-ray linear dichroism (XLD) for x-ray absorption spectroscopy (XAS) and RIXS are ideal tools to detect electronic anisotropy in such systems with charge and orbital

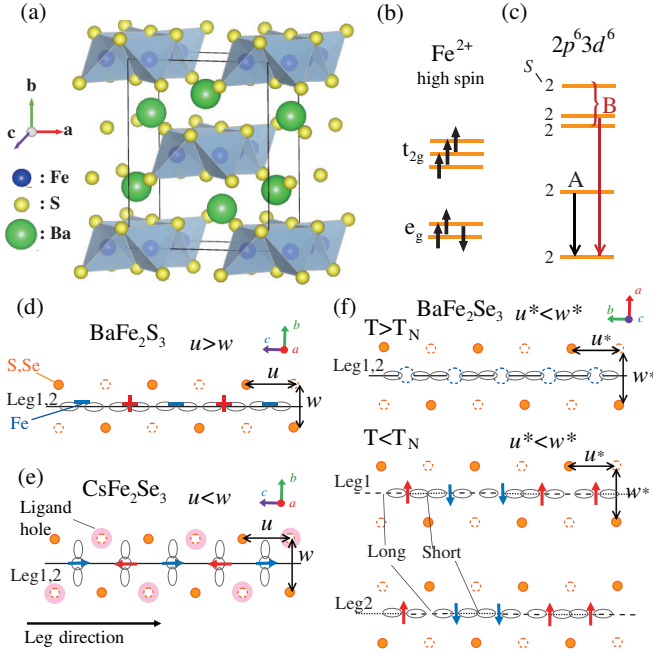


FIG. 1. (Color online) Crystal and electronic structure of BaFe₂X₃ and CsFe₂Se₃. (a) Crystal structure of BaFe₂S₃ visualized using the software package Vesta [38]. (b) Electronic configuration of Fe²⁺ high-spin state in a tetrahedral symmetry. (c) Multiplet levels of the initial state for $2p^6 3d^6$ suggested in Ref. [21]. The Coulomb and crystal field interactions are considered with associated S number. A and B mark the two dominant $d-d$ excitation peaks seen in the RIXS experiment. (d),(e),(f) Schematic drawing of the magnetic structure and lattice distortion in a leg of Fe ladder for (d) BaFe₂S₃, (e) CsFe₂Se₃, and (f) BaFe₂Se₃, viewed from a side of the ladder. The definitions of crystal axes are different between BaFe₂S₃, CsFe₂Se₃, and BaFe₂Se₃. The S or Se layers locate up (solid circle) and down (dotted circle) the Fe-leg layer and consist Fe(S,Se)₄ tetrahedra. Gray lobes indicate examples of occupied orbitals. Magenta shades in (e) indicate the ligand holes suggested in Ref. [22].

degrees of freedom of transition-metal $3d$ electrons.

In the present article, we investigate electronic structures of BaFe₂S₃, BaFe₂Se₃, and CsFe₂Se₃ in the Fe sites by means of XAS and RIXS at the Fe $L_{2,3}$ absorption edges. An opposite XLD is observed for BaFe₂X₃ and CsFe₂Se₃, indicating the existence of the orbital order or fluctuation above Néel temperature (T_N). The orbital and AF order along the legs of Fe-ladder is emerged via the direct exchange interaction between the Fe sites in BaFe₂S₃. On the other hand, the molecular orbital formation along the rung is associated in CsFe₂Se₃.

Single crystals of BaFe₂S₃, BaFe₂Se₃, and CsFe₂Se₃ were grown by the melt-growth method [15, 20]. XAS and RIXS measurements were performed at the REIXS beamline of the Canadian Light Source [26]. The single crystals were cleaved at room temperature (300 K) under the base pressure of 5×10^{-6} Pa for the XAS and RIXS measurements. The cleaved surfaces were oriented to the

(110) planes for BaFe₂S₃ and CsFe₂Se₃, and (100) plane for BaFe₂Se₃, parallel to the legs of ladder. Although the crystals of BaFe₂Se₃ consist of some blocks misaligned by a rotation along the ladder direction [11, 21], this fact does not seriously affect the main conclusion of XLD for $E // \text{leg}$ or $E \perp \text{leg}$ discussed later. The XAS spectra were recorded both in the total-electron-yield (TEY) and total-fluorescence-yield (TFY) modes. At the RIXS measurement, the samples were measured at the incident angle of 60° and the emission was detected at $\theta = 90^\circ$ for the x-ray [See inset of Fig. 4 (d) about the experimental geometry]. The beamline slit was set to $25 \mu\text{m}$, which resulted in an effective combined resolution of both the incoming beam and spectrometer of ~ 0.8 eV for RIXS measurements at the Fe L_3 edge. The energy of outgoing photons was calibrated by a reflection from a copper plate.

Figure 2 shows the XAS spectra at the Fe $L_{2,3}$ absorption edge of BaFe₂S₃, BaFe₂Se₃, and CsFe₂Se₃ taken with the (a) TEY and (b) TFY modes at room-temperature. Spectral difference between the less-distorted TEY and bulk-sensitive TFY spectra is barely observed, indicating the clean ordered surface for these samples. The two white lines in the spectra result from $2p$ to $3d$ dipole transitions ($2p^6 3d^6 \rightarrow 2p^5 3d^7$) with the well-separated spin-orbit-split $2p$ states $2p_{3/2}$ (L_3) and $2p_{1/2}$ (L_2), appearing respectively at around ~ 708 and ~ 721 eV. No sharp multiplet is observed in the spectra, that exhibits a similar spectral shape as Fe-chalcogenides of Fe(S,Te) [27] and Fe-pnictide materials [28–32]. Additionally, some spectral weights can be seen in the energy range of 3–5 eV above the white lines. These features are an indication of interaction of the chalcogen sites with the Fe $3d$ states [27] and is notably well-separated in the sharp spectrum for CsFe₂Se₃. Despite the formal Fe valence of $+2.5$ for CsFe₂Se₃, the spectrum of CsFe₂Se₃ is very sharp but consistent with the observation of a previous Fe $2p$ XPS study [22], indicating a localized Mott insulating nature with Fe²⁺. If all the Fe sites in CsFe₂Se₃ take the high-spin Fe²⁺ configuration, the extra positive charge ($+0.5$ per Fe) should be located at the Se sites.

On the other hand, some shoulder structures below the white lines are observed in the spectra of BaFe₂S₃ and BaFe₂Se₃, that are also similar to the Fe $2p$ XPS spectra and corresponding to rather electron doping compared to the case of CsFe₂Se₃. In Fig. 2(a), the results of Mahan's-line shape fitting are indicated by the dashed curves. The weak but significant components are observed at the pre-edge region ~ 1.0 eV below the white lines for BaFe₂Se₃ and BaFe₂S₃. On the XPS study, these two components have been ascribed as the contribution from itinerant and localized electrons. Probably, the low energy structure for XAS originate from the itinerant e_g empty state of the Fe²⁺ high-spin state [See Fig.1 (c)]. The itinerant and localized electrons will coexist in BaFe₂Se₃ and BaFe₂S₃. The Fe $3d$ electrons

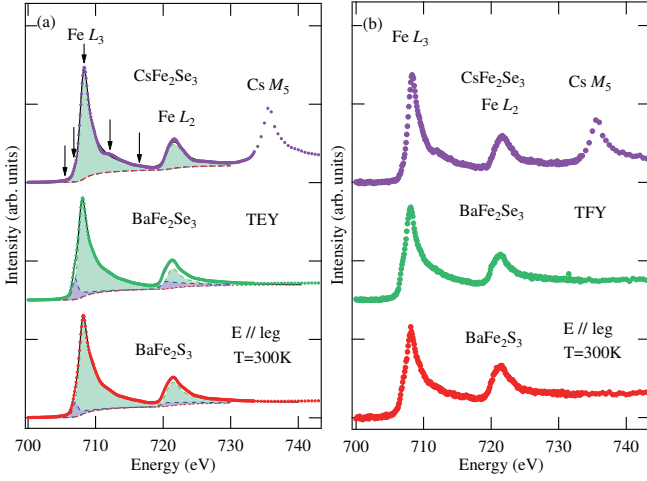


FIG. 2. (Color online) XAS spectra at the Fe $L_{2,3}$ edges for BaFe_2X_3 ($X = \text{S}$ and Se) and CsFe_2Se_3 taken in the (a) TEY and (b) TFY modes. The dashed lines indicate the results of curve fitting. The arrows indicate the incident energies used in the RIXS measurements shown in Fig. 4.

with the Fe^{2+} high-spin configuration and the Se $4p$ (or S $3p$) holes are localized in CsFe_2Se_3 , whereas they are partially delocalized in BaFe_2Se_3 and BaFe_2S_3 .

Figure 3 gives the XLD spectra of BaFe_2X_3 ($X = \text{S}$ and Se) and CsFe_2Se_3 at room temperature. The spectra are normalized by the area between 700 eV and 730 eV. The substantial XLD ($I_{E//\text{leg}} - I_{E\perp\text{leg}}$) is observed for all samples and exhibit an opposite behaviour for BaFe_2X_3 and CsFe_2Se_3 . The sign of XLD is minus for BaFe_2S_3 below the L_3 main peak of 708.1 eV in the overall pre-edge region and plus in the higher energy region. XLD observed in the spectra for BaFe_2S_3 is fairly similar to that obtained for BaFe_2As_2 ($I_{AF} - I_{\text{ferromagnetic}}$) below the structural transition T_s [32]. XLD for BaFe_2As_2 was consistent with the existence of an orbital order along their AF direction and an opposite to tendency of their local structural distortion of $a_{AF} > b_{\text{ferromagnetic}}$ [33]. The spectrum for BaFe_2S_3 in the pre-edge region taken with the $E//\text{leg}$ ($E \perp \text{leg}$) polarization detects the empty e_g state of the $d_{3z^2-r^2}$ ($d_{x^2-y^2}$) orbital. Here, z is defined to be parallel to the leg direction, or c for BaFe_2S_3 and CsFe_2Se_3 , and b for BaFe_2Se_3 , respectively. In addition, the FeS_4 tetrahedra in the two-leg ladder of BaFe_2S_3 are elongated along the leg direction ($u/w \sim 1.03$) [10], and the local structural distortion is opposite to the sign of XLD as similar to the case of BaFe_2As_2 [See Fig. 1(d)]. Therefore, $d_{3z^2-r^2}$ is occupied and the orbital order along the leg direction is indicated in BaFe_2S_3 even above T_N . The direct exchange between the $d_{3z^2-r^2}$ orbitals seems to stabilize the simple AF striped order below T_N for BaFe_2S_3 .

In the case of BaFe_2Se_3 , most of the $d_{3z^2-r^2}$ orbitals should be occupied, since its XLD is essentially similar to that of BaFe_2S_3 . However, there is a dip-hump like

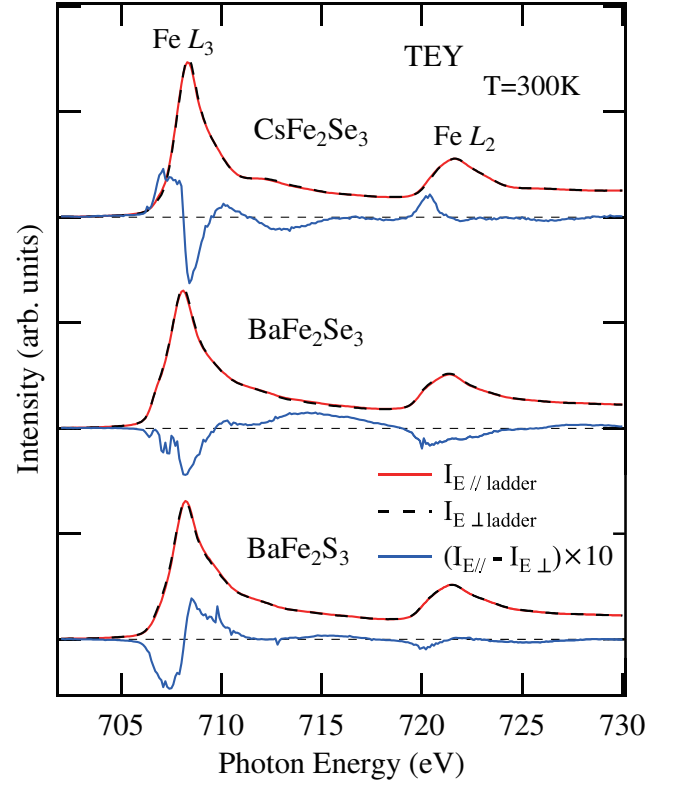


FIG. 3. (Color online) XAS spectra at the Fe $L_{2,3}$ edges for BaFe_2X_3 ($X = \text{S}$ and Se) and CsFe_2Se_3 with two different polarizations taken in the TEY modes at $T = 300$ K. The blue curves are the XLD spectra.

shape in the pre-edge region of ~ 707 eV and the average lengths between the Se sites exhibits $u^* < w^*$ above T_N in contrast to BaFe_2S_3 [10]. The small Fe vacancy will affects the electronic configuration for BaFe_2Se_3 and the orbital order may become more complicated, corresponding to their block-type magnetism and lattice distortion below T_N .

On the other hand, there is a peak in the pre-edge region of XLD for CsFe_2Se_3 and it exhibits a dip at the main-peak structure around 708.4 eV. In addition, the FeSe_4 tetrahedra of CsFe_2Se_3 are compressed ($u/w \sim 0.98$) along the leg [15]. Therefore, more holes are suggested in the $d_{3z^2-r^2}$ orbital rather than in the $d_{x^2-y^2}$. Namely, the orbital order perpendicular to the leg direction is indicated in CsFe_2Se_3 , in contrast to BaFe_2S_3 [See also Fig. 1(e)]. However, the very sharp Fe peaks with the satellite-like structures of CsFe_2Se_3 cannot be simply understood for the formal valence of 2.5+ with any kind of the orbital order in the Fe sites, whereas this observation is still consistent with the insulating nature of this compound.

In order to examine the energy levels in the Fe sites, RIXS spectra have been acquired for incident energies $h\nu_i$ across the Fe L_3 -edge XAS spectra as indicated by the arrows in Fig. 2(a). The data are shown in Fig. 4

for (a) BaFe_2S_3 , (b) BaFe_2Se_3 , and (c) CsFe_2Se_3 , respectively, on an energy loss scale $\hbar\Omega = h\nu_f - h\nu_i$, where $h\nu_f$ is the energy of outgoing photons. Although some elastic lines are observed at zero energy loss taken with the vertical polarization, these are barely observed on the spectra with horizontal polarization owing to the experimental geometry given in the inset of Fig. 4(d). The strong fluorescence indicated by the blue arrows are observed on the spectra with $h\nu_i > 706.8$ eV and disperses from 1 eV energy loss to higher energy losses, which was ascribed by the hybridization effects between Fe $3d$ states and Se $4p$ states in the high-resolution study for BaFe_2Se_3 by Monney *et al.* [21]. The fluorescence contributions shift to higher energy losses for increasing incident energies, as fluorescence in RIXS typically occurs at fixed x-ray emission energy. Monney *et al.* also suggested two Raman-like peaks labeled as A and B, not moving in energy position with variation of incident photon energy, superimposed on top of the fluorescence, which are clearly seen in the spectra with $h\nu_i = 705.5$ eV zoomed in Fig. 4 (d). These two Raman-like peaks A and B are corresponding to the energy of $d-d$ excitations in the Fe sites [See Fig. 1(c)]. The peak energies of A roughly correspond to the magnitude of band gap and increase in going from 0.4 eV for BaFe_2S_3 , 0.8 eV for BaFe_2Se_3 , to 1.3 eV for CsFe_2Se_3 , which are more or less consistent with the order for the activation energies [19, 20] and threshold energies of the photoemission spectroscopy [22].

The orbital order perpendicular to the leg direction and the relatively large band gap in CsFe_2Se_3 can be explained by the molecular orbital formation between the two Fe sites of the rung, namely ferromagnetic dimer formation [34, 35]. In this scenario, the bonding orbital accommodates two electrons of the e_g states in the two Fe sites across the rung in CsFe_2Se_3 and the gap is opened between the bonding and anti-bonding states. Since the $d_{x^2-y^2}$ orbitals along the rung become a bonding localized state, the $d-d$ excitation of A on RIXS with the vertical polarization and $I_{E//\text{leg}}$ of the pre-edges on XLD are enhanced. On the other hand, the ferromagnetic dimers are destabilized partially in BaFe_2Se_3 and completely in BaFe_2S_3 and then $I_{E\perp\text{leg}}$ of XLD are enhanced. The gap sizes depend on the transfer between the dimers and therefore become very small in BaFe_2X_3 . This scenario seems to be consistent with a recent inelastic neutron scattering study for BaFe_2S_3 [36]. It indicates a strong intra-ladder ferromagnetic exchange interaction along the rung direction, although BaFe_2S_3 still exhibits the commonly striped AF spin excitations. In addition, the importance of Hund's rule coupling has generally been suggested in iron-based superconductors, which leads to ferromagnetic interaction between the itinerant electrons and local moments [37]. Therefore, the present results indicate that a wider range of interactions, namely ferromagnetic and AF interactions originated from the orbital degeneracy, may result in superconductivity of these sys-

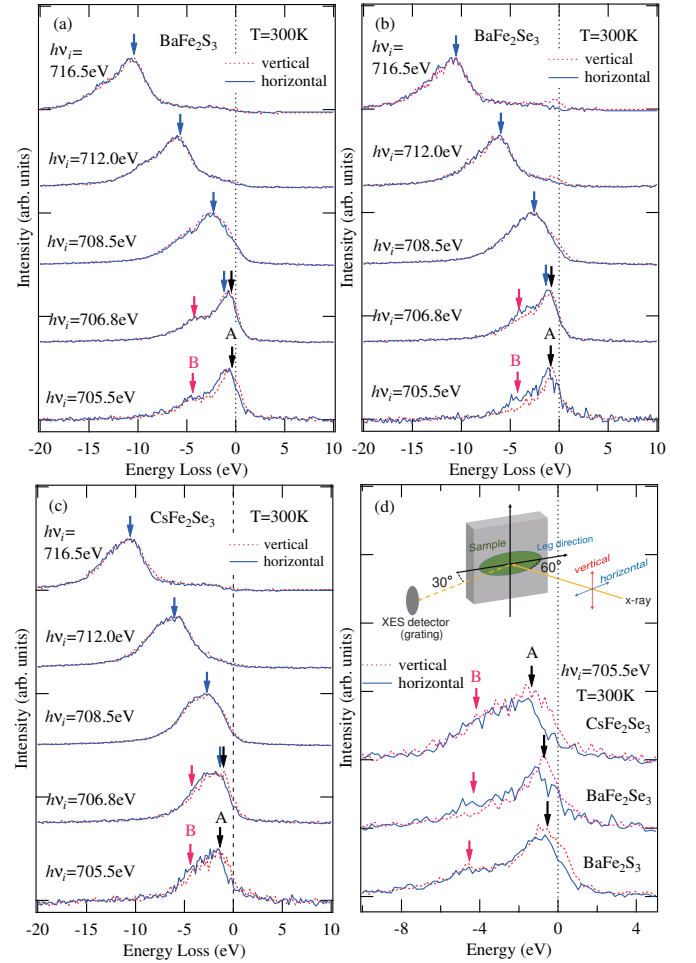


FIG. 4. (Color online) RIXS spectra measured with selected incident energies at the Fe L_3 edge for (a) BaFe_2S_3 , (b) BaFe_2Se_3 , and (c) CsFe_2Se_3 at $T = 300$ K. The blue arrows indicate the contribution from the fluorescence. The black and red arrows indicate Raman-like peaks labelled as A and B. (d) RIXS spectra with $h\nu = 705.5$ eV, zoomed into the low-energy-loss region. The inset shows the experimental geometry of RIXS.

tems.

In conclusion, we have studied the electronic structures of BaFe_2X_3 ($X = \text{S}$ and Se) and CsFe_2Se_3 using x-ray absorption and resonant inelastic x-ray scattering spectroscopy. XAS peak structure at the Fe L edges consists of the two components in BaFe_2X_3 , indicating that the itinerant and localized Fe $3d$ electrons coexist. On the other hand, the sharp peak at Fe L edges for CsFe_2Se_3 exhibit the single component accompanied with the well separated charge-transfer like satellite. XLD indicates that the different type of the orbital order occurs in BaFe_2X_3 and CsFe_2Se_3 above T_N , which originate from the direct exchange between the $d_{3z^2-r^2}$ orbitals and molecular orbital formation bridging the rungs, respectively.

The authors thank Dr. D. Ootsuki and Dr. Y. Hirata

for valuable discussions. Research described in this paper was performed at the Canadian Light Source, which is supported by the Canada Foundation for Innovation, Natural Sciences and Engineering Research Council of Canada, the University of Saskatchewan, the Government of Saskatchewan, Western Economic Diversification Canada, the National Research Council Canada, and the Canadian Institutes of Health Research. This work was supported by the Japan Society for the Promotion of Science (JSPS) of Grant-in-Aid for Young Scientists (B) (No. 16K20997) and for Scientific Research (B) (No. 16H04019). This work was also partially supported by Ministry of Education, Culture, Sports, Science, and Technology of Japan (X-ray Free Electron Laser Priority Strategy Program).

* ktakubo@issp.u-tokyo.ac.jp

- [1] I. I. Mazin, D. J. Singh, M. D. Johannes, and M. H. Du, *Phys. Rev. Lett.* **101**, 05700 (2008).
- [2] K. Kuroki, S. Onari, R. Arita, H. Usui, Y. Tanaka, H. Kontani, and H. Aoki, *Phys. Rev. Lett.* **101**, 087004 (2008).
- [3] C.-C. Lee, W.-G. Yin, and W. Ku, *Phys. Rev. Lett.* **103**, 267001 (2009).
- [4] P. Dai, *Rev. Mod. Phys.* **87**, 855 (2015).
- [5] Y. Yamakawa, S. Onari, and H. Kontani, *Phys. Rev. X* **6**, 021032 (2016).
- [6] A. V. Chubukov, M. Khodas, and R. M. Fernandes, *Phys. Rev. X* **6**, 041045 (2016).
- [7] J. Guo, S. Jin, G. Wang, S. Wang, K. Zhu, T. Zhou, M. He, and X. Chen, *Phys. Rev. B* **82**, 180520 (2010).
- [8] Z. Shermadini, A. Krzton-Maziopa, M. Bendele, R. Khasanov, H. Luetkens, K. Conder, E. Pomjakushina, S. Weyeneth, V. Pomjakushin, O. Bossen, and A. Amato, *Phys. Rev. Lett.* **106**, 117602 (2011).
- [9] F. Ye, S. Chi, W. Bao, X. F. Wang, J. J. Ying, X. H. Chen, H. D. Wang, C. H. Dong, and M. Fang, *Phys. Rev. Lett.* **107**, 137003 (2011).
- [10] H. Hong and H. Steinfink, *J. Solid State Chem.* **5**, 93 (1972).
- [11] A. Krzton-Maziopa, E. Pomjakushina, V. Pomjakushin, D. Sheptyakov, D. Chernyshov, V. Svitlyk, and K. Conder, *J. Phys.: Condens. Matter* **23**, 402201 (2011).
- [12] J. M. Caron, J. R. Neilson, D. C. Miller, A. Llobet, and T. M. McQueen, *Phys. Rev. B* **84**, 180409 (2011).
- [13] J. M. Caron, J. R. Neilson, D. C. Miller, K. Arpino, A. Llobet, and T. M. McQueen, *Phys. Rev. B* **85**, 180405 (2012).
- [14] Y. Nambu, K. Ohgushi, S. Suzuki, F. Du, M. Avdeev, Y. Uwatoko, K. Munakata, H. Fukazawa, S. Chi, Y. Ueda, and T. J. Sato, *Phys. Rev. B* **85**, 064413 (2012).
- [15] F. Du, K. Ohgushi, Y. Nambu, T. Kawakami, M. Avdeev, Y. Hirata, Y. Watanabe, T. J. Sato, and Y. Ueda, *Phys. Rev. B* **85**, 214436 (2012).
- [16] S. Chi, Y. Uwatoko, H. Cao, Y. Hirata, K. Hashizume, T. Aoyama, and K. Ohgushi, *Phys. Rev. Lett.* **117**, 047003 (2016).
- [17] H. Takahashi, A. Sugimoto, Y. Nambu, T. Yamauchi, Y. Hirata, T. Kawakami, M. Avdeev, K. Matsubayashi, F. Du, C. Kawashima, H. Soeda, S. Nakano, Y. Uwatoko, Y. Ueda, T. J. Sato, and K. Ohgushi, *Nat. Mater.* **14**, 1008 (2015).
- [18] T. Yamauchi, Y. Hirata, Y. Ueda, and K. Ohgushi, *Phys. Rev. Lett.* **115**, 246402 (2015).
- [19] H. Lei, H. Ryu, A. I. Frenkel, and C. Petrovic, *Phys. Rev. B* **84**, 214511 (2011).
- [20] Y. Hirata, S. Maki, J. I. Yamaura, T. Yamauchi, and K. Ohgushi, *Phys. Rev. B* **92**, 205109 (2015).
- [21] C. Monney, A. Uldry, K. J. Zhou, A. Krzton-Maziopa, E. Pomjakushina, V. N. Strocov, B. Delley, and T. Schmitt, *Phys. Rev. B* **88**, 165103 (2013).
- [22] D. Ootsuki, N. L. Saini, F. Du, Y. Hirata, K. Ohgushi, Y. Ueda, and T. Mizokawa, *Phys. Rev. B* **91**, 014505 (2015).
- [23] Q. Luo, A. Nicholson, J. Rincon, S. Liang, J. Riera, G. Alvarez, L. Wang, W. Ku, G. D. Samolyuk, A. Moreo, and E. Dagotto, *Phys. Rev. B* **87**, 024404 (2013).
- [24] S. Dong, J.-M. Liu, and E. Dagotto, *Phys. Rev. Lett.* **113**, 187204 (2014).
- [25] Z. V. Popović, M. Šćepanović, N. Lazarević, and M. Opačić, M. M. Radonjić, D. Tanasković, *Phys. Rev. B* **91**, 064303 (2015).
- [26] D. G. Hawthorn, F. He, L. Venema, H. Davis, A. J. Achkar, J. Zhang, R. Sutarto, H. Wadati, A. Radi, T. Wilson, G. Wright, K. M. Shen, J. Geck, H. Zhang, V. Novk, and G. A. Sawatzky, *Rev. Sci. Instrum.* **82**, 073104 (2011).
- [27] N. L. Saini, Y. Wakisaka, B. Joseph, A. Iadecola, S. Dalela, P. Srivastava, E. Magnano, M. Malvestuto, Y. Mizuguchi, Y. Takano, T. Mizokawa, and K. B. Garg, *Phys. Rev. B* **83**, 052502 (2011).
- [28] W. L. Yang, A. P. Sorini, C.-C. Chen, B. Moritz, W.-S. Lee, F. Vernay, P. Olalde Velasco, J. D. Denlinger, B. Delley, J.-H. Chu, J. G. Analytis, I. R. Fisher, Z. A. Ren, J. Yang, W. Lu, Z. X. Zhao, J. van den Brink, Z. Hussain, Z.-X. Shen, and T. P. Devereaux, *Phys. Rev. B* **80**, 014508 (2009).
- [29] C. Parks Cheney, F. Bondino, T. A. Callcott, P. Vilmercati, D. Ederer, E. Magnano, M. Malvestuto, F. Parmigiani, A. S. Sefat, M. A. McGuire, R. Jin, B. C. Sales, D. Mandrus, D. J. Singh, J. W. Freeland, and N. Mannella, *Phys. Rev. B* **81**, 104518 (2010).
- [30] F. Bondino, E. Magnano, M. Malvestuto, F. Parmigiani, M. A. McGuire, A. S. Sefat, B. C. Sales, R. Jin, D. Mandrus, E. W. Plummer, D. J. Singh, and N. Mannella, *Phys. Rev. Lett.* **101**, 267001 (2008).
- [31] F. Bondino, E. Magnano, C. H. Booth, F. Offi, G. Panaccione, M. Malvestuto, G. Paolicelli, L. Simonelli, F. Parmigiani, M. A. McGuire, A. S. Sefat, B. C. Sales, R. Jin, P. Vilmercati, D. Mandrus, D. J. Singh, and N. Mannella, *Phys. Rev. B* **82**, 014529 (2010).
- [32] Y. K. Kim, W. S. Jung, G. R. Han, K.-Y. Choi, C.-C. Chen, T. P. Devereaux, A. Chainani, J. Miyawaki, Y. Takata, Y. Tanaka, M. Oura, S. Shin, A. P. Singh, H. G. Lee, J.-Y. Kim, and C. Kim, *Phys. Rev. Lett.* **111**, 217001 (2013).
- [33] C.-C. Chen, J. Maciejko, A. P. Sorini, B. Moritz, R. R. P. Singh, and T. P. Devereaux, *Phys. Rev. B* **82**, 100504(R) (2010).
- [34] V. Pardo, S. Blanco-Canosa, F. Rivadulla, D. I. Khomskii, D. Baldomir, Hua Wu, and J. Rivas, *Phys. Rev. Lett.* **101**, 256403 (2008).
- [35] I. I. Mazin, H. O. Jeschke, K. Foyevtsova, R. Valent, and

- D. I. Khomskii, Phys. Rev. Lett. **109**, 197201 (2012).
- [36] M. Wang, S. J. Jin, M. Yi, Y. Song, H. C. Jiang, W. L. Zhang, H. L. Sun, H. Q. Luo, A. D. Christianson, E. Bourret-Courchesne, D. H. Lee, D.-X. Yao, and R. J. Birgeneau Phys. Rev. B **95**, 060502(R) (2017).
- [37] K. Haule and G. Kotliar, New J. Phys. **11** 025021 (2009).
- [38] K. Homma and F. Izumi, J. Appl. Crystallogr. **44**, 1272 (2011).